Journal of The
Electrochemical Society

The Effect of Metallographic Preparation on the Surface Characteristics and Corrosion Behaviour of Ti-6Al-4V Alloy in Simulated Physiological Solutions

To cite this article: Ingrid Milošev *et al* 2024 *J. Electrochem. Soc.* **171** 111503

Journal of The Electrochemical Society, 2024 **171** 111503

The Effect of Metallographic Preparation on the Surface Characteristics and Corrosion Behaviour of Ti-6Al-4V Alloy in Simulated Physiological Solutions

Ingrid Milošev,[1,2,*,z] Denis Sačer,[1] Barbara Kapun,[1] and Peter Rodič[1]

[1]*Jožef Stefan Institute, Department of Physical and Organic Chemistry, SI-1000 Ljubljana, Slovenia*
[2]*Valdoltra Orthopaedic Hospital, SI-6280 Ankaran, Slovenia*

This study aimed to determine the effect of surface metallographic preparation (grinding, diamond polishing, and chemo-mechanical polishing using silica and hydrogen peroxide) on the surface roughness, morphology, chemical composition, and electrochemical behaviour of Ti-6Al-4V alloy. Roughness decreases from ca. 0.2 μm to 0.02 μm from grinding to polishing. A typical $\alpha+\beta$ microstructure can be observed only after chemo-mechanical polishing. The average composition of ca. 6 wt% Al, 4 wt% V, and rest Ti was determined regardless of the surface preparation. X-ray photoelectron spectroscopy revealed that the thickness of the oxide layer formed on chemo-mechanical polished samples is half that of ground samples. The metallographic preparation largely affects the corrosion behaviour of Ti-6Al-4V, which was investigated using electrochemical impedance spectroscopy and potentiodynamic polarisation in 0.9 wt% NaCl and artificial saliva at 37°C. At the open circuit potential, the chemo-mechanically polished Ti-6Al-4 samples showed superior corrosion resistance over ground samples. At potentials over 2.5 V vs Ag/AgCl, increased current densities were noted for chemo-mechanically polished samples, presumably related to the oxidation to a thicker oxide.

 [DOI: 10.1149/1945-7111/ad8e89]

Manuscript submitted August 14, 2024; revised manuscript received October 31, 2024. Published November 13, 2024.

Supplementary material for this article is available online

Titanium (Ti) and its alloys are extensively used in the aviation industry,[1–3] biomedical field,[4–8] marine[9,10] and many other industries[11] owing to their exceptional mechanical and electrochemical properties, coupled with low biotoxicity. The spontaneous development of protective titanium oxide (TiO_2) layers on the surface of Ti-based materials contributes to their outstanding corrosion resistance.[12,13] In biomedical applications, the preference for Ti-6Al-4V over pure metallic Ti is driven by the enhanced mechanical properties of the alloy.[14] The microstructure of Ti-6Al-4V features both α (hcp, hexagonal close-packed) and β (bcp, body-centred cubic) phases, with Al stabilising the α phase and V stabilising the β phase. The microstructure of such a biphasic system consists of an α phase matrix appearing as elongated grains. In contrast, the β phase, which is V-rich, appears as equiaxed grains surrounded by α grains.[15]

In general, titanium alloys are, depending on the application, subject to various physical, chemical or biochemical treatments. Physical methods for preparing titanium surfaces involve techniques that utilise physical forces rather than chemical reactions to modify the surface properties, for example, physical vapour deposition[16,17] and ion implantation[18] aiming to enhance surface hardness, wear resistance, and biocompatibility and to modify surface morphology, texture, and surface chemistry. As an example of chemical treatment, the anodic oxidation of Ti-6Al-4V alloy results in the increased thickness of the TiO_2 layer and increased corrosion resistance.[19,20] A reduction of titanium dissolution in a saline electrolyte was achieved by boiling in water and thermal oxidation, ascribed to transforming the surface TiO_2 layer from the anatase form to the more compact rutile form.[21] Biochemical preparation of titanium surfaces for medical implant applications involves modifying the surface properties to improve biocompatibility, cell adhesion, and osseointegration.[22,23] Various techniques are employed to achieve this, often involving the creation of bioactive coatings or modifications that encourage favourable interactions with biological tissues, usually supported by surface roughening by sandblasting to promote osseointegration.[22]

The TiO_2 layer acts as a stable passive film adhered to the Ti surface, preventing further reaction between the underlying metal and the corrosive environment.[13,24–26] The exact composition and structure of the passive layer depend on various factors, including the specific environmental conditions and the electrochemical processes occurring at the titanium surface. Besides TiO_2, titanium can form suboxides, such as TiO and Ti_2O_3, depending on the specific conditions, like the pH of the solution and the potential applied to the titanium.[13,24–27]

The metallographic surface preparation of titanium surfaces includes grinding and polishing, to modify the surface texture and morphology according to specific requirements. Grinding helps smoothen the surface, while diamond polishing or silica and alumina polishing enhances its shine and removes any remaining imperfections. Metallographic chemical etching may follow grinding or polishing steps to visualise the microstructure. Metallographic preparation affects not only the roughness but also the chemical composition of the surface. In our previous study, the effect of surface preparation and treatment of Nitinol (Ni-Ti alloy) on the surface morphology, composition and electrochemical properties in simulated body fluid (SBF) was studied.[28,29] The surface roughness decreased from chemically etched over the ground to the polished surface. Distinct differences in the chemical composition of the outermost surface were observed: grinding led to the preferential removal of nickel and surface enrichment in titanium and titanium oxides (TiO_2 and Ti_2O_3). Polishing produced thinner oxide layers, which showed superior corrosion resistance in the simulated physiological solution.[28]

Several literature studies have addressed the effect of surface preparation of Ti alloys and presented experimental evidence that surface (metallographic) preparation can significantly impact the properties of the passive layer and its corrosion resistance. Surface finishing and shape effects (convex, concave and flat) on corrosion resistance of Ti-6Al-4V alloy were investigated.[30] The combination of polished surface (3 μm alumina paste) and convex shape showed the best electrochemical passive behaviour of the Ti-6Al-4V sample in SBF compared to SiC papers-ground and concave-shaped samples.[30] Electrochemical behaviour in Fusayama Meyer saliva for as-received Ti-6Al-4V samples differed from that of polished samples prepared by grinding and polishing with diamond paste and

*Electrochemical Society Member.
[z]E-mail: ingrid.milosev@ijs.si

colloidal silica solution.[31] Lower roughness achieved by polishing improved the corrosion properties of the alloy, while the rougher, as-received samples showed an increased pitting susceptibility. Similar results were noticed by Chi et al., who investigated the electrochemical properties of Ti-6Al-4V in 12 wt% HCl at 35 °C, simulating harsh conditions in oil and gas industries.[32] The samples ground and polished using silica suspension showed lower pit growth rate and pitting corrosion susceptibility than abraded (ground) samples.[32] The corrosion resistance of titanium samples made using different fabrication methods (cast or machining) subject to sandblasting (600-grit SiC papers) and polishing (50 μm alumina particles) was compared.[33] Potentiodynamic polarisation curves measured in artificial saliva showed that the current densities were smaller for polished samples. Similar results were reported for the micro-rough surface of Ti, which has better corrosion resistance and lower ion release than the macro-rough surface.[34] It was hypothesised that a less rough surface with improved structural uniformity facilitates the formation of ordered, compact surface protective film.[34]

Contrary to the listed references, where the polishing beneficially affected the electrochemical response of Ti and Ti-6Al-4V over grinding, Cheng and Roscoe reported that the 1 μm-diamond polishing of CP Ti deteriorated the corrosion stability of the passive film formed in phosphate buffer saline.[35] A sharp increase in current density was observed at potentials above 2 V, indicating that the passive film is less protective than that formed on SiC-ground samples. The formation of bubbles accompanied significantly higher current densities observed for polished samples. However, no crevices, pits or other localised features were observed.[35]

Along with the mechanical steps of grinding and polishing the Ti and Ti alloy surfaces, a chemo-mechanical procedure is often used to clean or remove the protective oxide layer and expose the underlying substrate. Chemical mechanical polishing (CMP) (or chemical mechanical planarisation) is smoothing surfaces with chemical and mechanical forces, usually chemical etching and free abrasive polishing. The typical slurry consists of a nano-sized abrasive, typically colloidal silica (SiO_2) or alumina (Al_2O_3), and chemical etchant like hydrogen peroxide. This combination of chemical and mechanical material processing enables the uniform removal rate and smoothening (planarisation) of the surface.

Several studies addressed the CMP of Ti alloys; however, discrepancies in interpretations were observed, and due to various experimental parameters, it is difficult to draw straightforward conclusions. CMP of Ti-6Al-4V was conducted in slurries consisting of 0.1 wt% EDTA-2Na as a chelating agent, 20 wt% colloidal silica and different percentages of H_2O_2 (0–5 wt%) with pH adjusted at 9.5.[36] Increasing H_2O_2 concentration led to larger corrosion currents reflecting enhanced metal dissolution.[36] It was also reported that 0.05 wt% H_2O_2 added to the slurry helped the rapid formation of TiO_2 on Ti and Ti-6Al-4V alloy, whereas, at higher concentrations, the corrosion properties deteriorated.[37] Slurries prepared by mixing 5 wt% alumina abrasives suspended in nitric acid at pH 4 to control the surface roughness and oxide thickness on Ti.[38] Induced optimal nano-scale roughness was reported to limit bacteria growth and enhance cell attachment.[38] The effects of different pH values and H_2O_2 content of the slurry containing 50 wt% silica and malic acid on the polishing process of the Ti-6Al-4V surface were studied.[39] The optimal pH of the slurry for polishing was determined to be 4, containing 8.3 wt% H_2O_2. This slurry produced a prominent increase in the dissolution of Ti, which is the aim of the CMP process. Further, it was noticed that basic slurry induced a higher removal rate than acidic slurry, creating a mirror-polished surface of Ti metal.[40]

The literature summary indicates a lack of a systematic study investigating the effect of surface metallographic preparation of Ti-6Al-4V on the roughness, composition, microstructure and electrochemical response in simulated physiological solutions. Discrepancies in the literature are presumably related to the different surface preparation methods. In none of the studies, samples that were prepared differently were comparatively studied using profilometry, surface analysis, and electrochemical measurements. It was noticed that the surface composition of Ti was affected by H_2O_2 in the slurry,[36–40] but the exact changes in composition as a function of surface preparation remain to be elucidated. Aiming to contribute to clarifying the effect of surface preparation, the effects of surface metallographic preparation were studied systematically from grinding over diamond polishing and chemo-mechanical polishing. The effect on microstructure, roughness and electrochemical properties was investigated using 3D profilometry, atomic force microscopy (AFM), scanning electron microscopy (SEM) combined with energy dispersive X-ray spectroscopy (EDXS), X-ray photoelectron spectroscopy (XPS) and potentiodynamic and impedance electrochemical measurements in two simulated physiological solutions (0.9 wt% NaCl and artificial saliva).

Experimental

Materials and chemicals.—As substrate material, commercially available Ti-6Al-4V alloy Grade 5 (ASTM B265) supplied by GoodFellow Ltd, (Cambridge, U.K.) was used. All measurements were performed on the samples cut from foil in discs (15 mm diameter, 2 mm thick). The surface of the samples was metallographically prepared on the LaboPol-20 grinding and polishing system equipped with a LaboForce-50 specimen mover unit (polishing head) supplied by Struers (Ballerup, Denmark). All other consumables, such as SiC emery papers, cloths and suspensions, were also purchased from Struers. The first group of samples was mechanically successively ground using 320, 500, 800, 1200, 2400, and 4000-grit SiC emery papers (Table I); specimens are denoted as Ti64-320, Ti64-1200, Ti64-2400 and Ti64-4000. The second group of samples was ground using 320-grit SiC papers and then polished with MD-Largo diamond suspension (DiaPro, 9 μm, Struers), denoted as Ti64-DP-L. The third group of samples was ground using 320-grit SiC papers, diamond polished using MD-Largo (DiaPro, 9 μm, Struers) and then chemo-mechanically polished (CMP) in the slurry containing the suspension of SiO_2, size

Table I. Details on metallographic preparation of Ti-6Al-4V samples and their designation.

Sample designation	Mechanically ground samples					
	#grit size (grain size)					
Ti64-320	#320 (46 μm)	—	—	—	—	—
Ti64-1200	#320 (46 μm)	#500 (30 μm)	#800 (22 μm)	#1200 (15 μm)	—	—
Ti64-2400	#320 (46 μm)	#500 (30 μm)	#800 (22 μm)	#1200 (15 μm)	#2400 (8 μm)	—
Ti64-4000	#320 (46 μm)	#500 (30 μm)	#800 (22 μm)	#1200 (15 μm)	#2400 (8 μm)	#4000 (5 μm)
	Diamond-polished samples					
Ti64-DP-L	#320 (46 μm)	diamond-polished MD Largo DiaPro (9 μm)				—
	Chemo-mechanically-polished (CMP) samples					
Ti64-OP-S	#320 (46 μm)	diamond-polished MD Largo DiaPro (9 μm)				chemo-mech. polished (SiO_2, 0.25 μm + 10% v/v H_2O_2)

0.04 μm (0.25 μm agglomerated) (OP-S, Struers) and 30% H_2O_2 (10% v/v, LabExpert Kefo d.o.o), pH = 9.8, according to Struers protocol; these samples and denoted as Ti64-OP-S. During polishing, the rotation speed was 150 rpm, and the force was 20 kN. In the final step, samples were ultrasonically cleaned with water, ethanol and acetone (both Carlo Erba Reagents) and dried in the air stream. Prepared samples were used for electrochemical measurements, roughness and surface analysis.

Electrochemical measurements were conducted in two solutions to simulate physiological conditions, such as those in the human body. The first set was conducted in 0.9 wt% NaCl (pH = 5.5). This concentration of sodium chloride in water is similar to the salinity of body fluids like blood and sweat. The second is artificial saliva, which simulates the conditions of the oral environment, particularly for testing the corrosion resistance and biocompatibility of dental materials, prosthetics, and implants. It contained 0.4 g/L NaCl (Fischer Scientific), 0.4 g l^{-1} KCl (Sigma Aldrich), 0.795 g l^{-1} $CaCl_2{\cdot}2H_2O$ (Sigma Aldrich), 0.78 g l^{-1} $Na_2HPO_4{\cdot}2H_2O$ (Sigma Aldrich), 0.005 g l^{-1} Na_2S (Fischer Scientific) and 1 g l^{-1} urea (Sigma Aldrich) dissolved in 1 l deionised water (pH 6.8). Solutions were prepared with deionised water (Milli Q Direct water, resistivity equal to or greater than 18.2 MΩ·cm at 25 °C and total organic carbon value below 5 ppb (Millipore, Billerica, MA, USA).

Electrochemical measurements.—Electrochemical measurements were performed in a custom-made polymethylmethacrylate three-electrode cell with a 250 ml volume. The cell was equipped with a thermostatic jacket. The sample was fixed to the cell with a holder, and the exposed sample surface (1 cm^2) served as the working electrode. The reference electrode was a saturated silver/silver chloride electrode (Ag/AgCl) with electrode potential E = 0.197 V vs standard hydrogen electrode, and a graphite rod with a diameter of 5 mm acted as a counter electrode. Measurements were conducted in cells thermostated at 37 ± 0.1 °C. Multipotentiostat/galvanostat Autolab PGSTAT M204 (Metrohm Autolab, Nova software 2.1.6, Utrecht, The Netherlands) was used for all electrochemical measurements.

Upon immersion, the sample was stabilised at the open-circuit potential (OCP) for 1.5 h. Electrochemical impedance spectroscopy (EIS) measurements were performed at the OCP in the frequency range from 100 kHz to 10 mHz at 10 cycles per decade and a sinusoidal voltage amplitude of ±10 mV (rms). For each sample, measurements were performed in at least triplicate. A representative measurement was chosen and presented in plots. Experimental data were fitted using Nova 2.1.6 software.

Immediately after EIS, potentiodynamic polarisation (PDP) curves were recorded using a scan rate of 1 mV s^{-1} starting at −0.1 V vs OCP up to 6.0 V. Electrochemical parameters (corrosion potential, E_{corr}, corrosion current density, j_{corr}) were determined from PDP curves using Nova 2.1.6 software. A representative measurement was chosen and presented in plots; mean values with standard deviations are given in tables.

3-D topography and surface analysis.—3-D topography was determined at the surface (1 mm × 1 mm) of samples using a Bruker DektakXT profilometer. The recording resolution was 0.167 μm/per point. The mean surface roughness (S_a) was determined, and a 3D map of samples was made using the Bruker Vision 64 and TalyMap Gold 6.2 software. The value presented is the average of three repeatable measurements.

Atomic force microscopy (AFM) imaging was conducted using a Park NX20 instrument (Park Systems) equipped with the software SmartScan™. The AFM images were obtained using an ACTA cantilever with a high resonant frequency and a backside reflective coating (Park Systems). The tip shape was pyramidal, with a radius of 6 nm, length 14 − 16 μm and frequency 300 kHz. The scan rate was 0.3 Hz, and the area scanned 20 μm × 20 μm and 5 μm × 5 μm. The images were recorded in a non-contact mode.

Scanning electron microscopy (SEM), imaging was performed using an FEI Helios 650 Nanolab instrument at 10kV beam acceleration voltage using an ICE detector of secondary electrons (SE) to obtain insights into the morphology of the surface. A circular back-scattered (CBS) detector for back-scattered electrons (BSE) was used to get information on the composition since they contrast areas with different chemical compositions. Along with SEM analysis, energy dispersion X-ray spectroscopy (EDXS) was conducted using an Oxford Instruments AZtec system with X-max SDD (50 mm^2) detector at 10 kV.

X-ray photoelectron spectroscopy (XPS) was performed on a TFA Physical Electronics Inc. spectrometer equipped with a hemispherical analyser. The vacuum during the analysis was around 10^{-9} mbar. All the spectra were acquired utilising a monochromatic Al Kα X-ray source (1486.6 eV) with an analysed area of 400 μm in diameter. Survey scan spectra were obtained at a pass energy of 187.9 eV, while the core level single peaks were measured at 29.4 eV with an energy step of 0.1 eV. The take-off emission angle normal to a sample surface was 45°. The binding energies (E_b) were calibrated by referencing the C 1 s photoelectron peak at 284.8 eV. Chemical composition was quantified using the MultiPak processing software (Version 8.1).

Depth profiles of the oxide layers were obtained at the sputtering rate of 1.0 nm min^{-1} deduced on an Al_2O_3 layer of known thickness deposited by atomic layer deposition. The LLS (Linear Least Square) fitting tool in the Multipak software was used to decompose the Ti 2p spectra from the profile into Ti-oxide and Ti-metallic spectra. The oxide layer thickness was determined at the intersection between the curves of metal and Ti-oxide in both profiles. The same procedure was used to decompose the Al 2p spectra.

Results and Discussion

3D topography, morphology and chemical composition of the Ti-6Al-4V samples subject to different metallographic preparations.—A decrease in surface roughness with increasing grit of SiC papers and/or polishing was commonly observed in literature for Ti and Ti-alloys[30,31,33,37–40] but no systematic data were reported for different grinding/polishing procedures. Figure 1 shows the surface 3D profiles of the alloy samples prepared using different grinding or polishing procedures. Progressively shallower abrading marks and smoother surfaces were formed with decreasing grit grain size of SiC papers. Roughness parameter S_a was obtained along the whole scanned area of the sample, i.e. 1 mm × 1 mm (Figs. 1a–1f). The values S_a are added in Fig. 1. The S_a decreased sharply from 0.243 μm for Ti64-320 to 0.098 μm for Ti64–1200. For Ti64–2400 and Ti64-4000, S_a was reduced to cca. 0.020 μm. A somewhat larger value (0.050 μm) was obtained for Ti64-DP-L than the Ti64-4000 sample due to the larger grain size (Table I). Ti64-OP-S exhibited the lowest surface roughness of 0.017 μm.

For representative samples, AFM imaging was used to analyse the surface topography and roughness at the smaller area units (20 μm × 20 μm and 5 μm × 5 μm area). The former images are presented in Fig. 2 and the latter in the Supplement (jesad8e89supp1.docx) (Fig. S1). Topographical features were much more profound when analysed using AFM at a smaller scale than 3D profilometry. Due to rough grinding, the Ti64-320 sample showed deep grooves with asperities along the edges. For the Ti64-2400 and Ti64-4000, the grooves were much shallower, leading to the progressive nivelling of the surface. The Ti64-OP-S exhibits a smooth surface with only a small number of asperities.

The deduced parameters of S_a are given in Fig. 2. S_a values were smaller than when determined using a 3D profilometer where the analysing area was 1 mm × 1 mm (Fig. 1).

The samples were further analysed using SEM/EDS analysis. Surface morphology of the Ti-6Al-4V samples after six different preparation procedures are shown in SEM images recorded using secondary electrons (Fig. 3). Following grinding with SiC papers, the surface consisted of randomly orientated longitudinal scratches

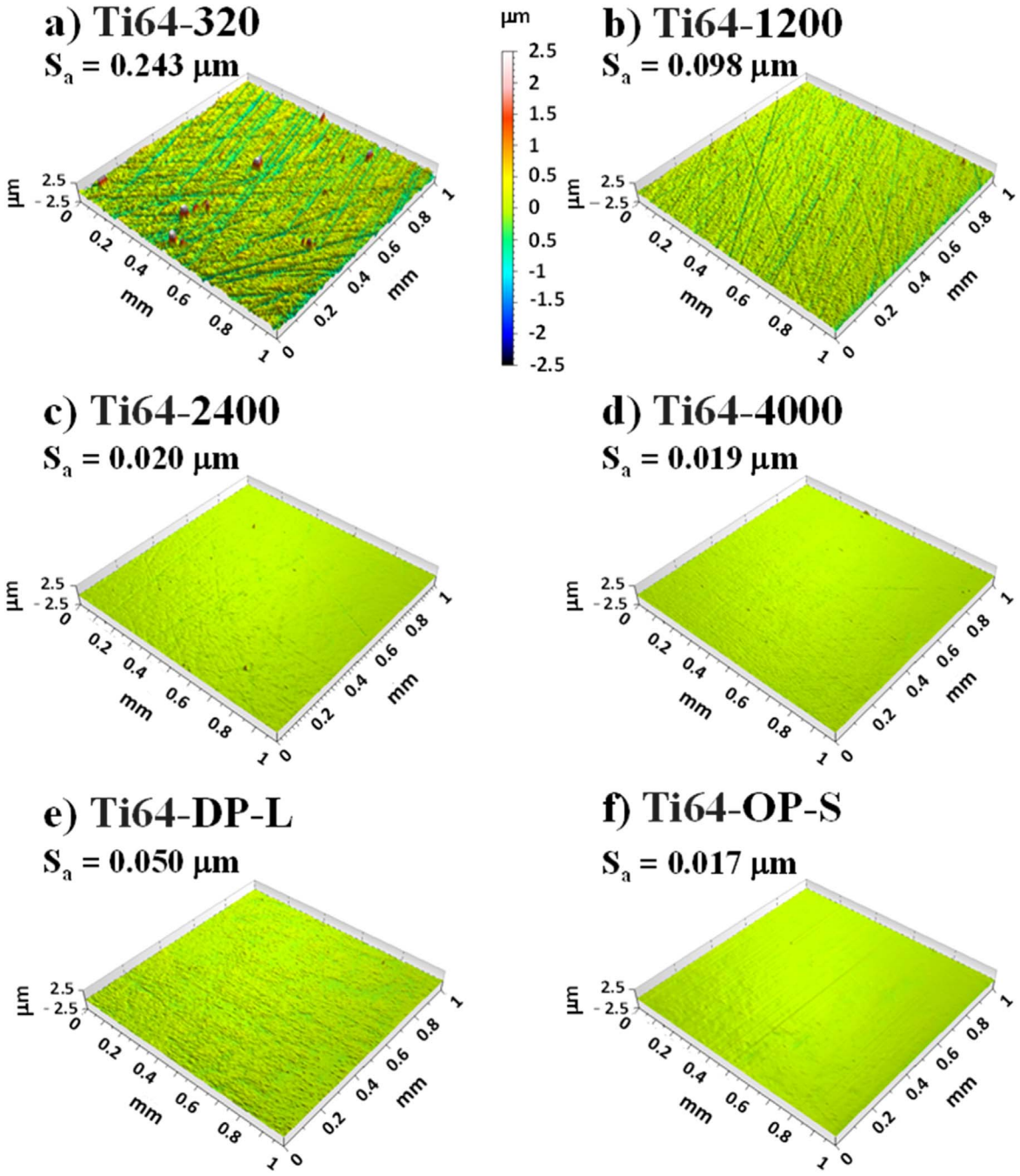

Figure 1. 3D surface topographies of Ti-6Al-4 V samples ground with SiC papers of (a) #320 grit, (b) #1200 grit, (c) #2400 grit, (d) #4000 grit, and (e) diamond-polished (Ti64-DP-L) and (f) chemo-mechanically polished (Ti64-OP-S). The S_a values are noted in the graph.

and ridges (Figs. 3a–3d). For the Ti64-320 sample, the abrading traces were broader, deeper and more profound than the Ti64-4000. The diamond-polished sample (Fig. 3e) showed fewer scratches and a smoother surface than Ti64-2400, albeit with similar grit size (9 µm and 8 µm, respectively, Table I). In contrast to the ground and diamond-polished samples, the typical $\alpha+\beta$ microstructure of the Ti64 alloy was visible for the Ti64-OP-S even on images made using secondary electrons (Fig. 3f).

Table II presents the results of the EDXS composition analysis as weight percentages of Ti, Al, V, O, and C. The analysis was made over all the areas imaged in Fig. 3. The Ti content ranged from 76.8% to 89.7% across all samples, consistent with titanium being a predominant element in the alloy composition. The Al and V contents exhibited slight variations among the samples but were around 6 wt% and 4 wt%, respectively, i.e. within expected compositional fluctuations. The carbon content was notably absent or negligible in most samples, indicating successful mitigation of carbon contamination during processing. The oxygen content demonstrated significant variability across the samples, ranging from 2.5% (Ti64-1200) to 12.1% (Ti64-2400). Only in Ti64-OP-S was no oxygen detected. Generally, the varying oxygen content may result from differences in processing conditions. Oxygen is typically considered an impurity in titanium alloys, and its presence can influence mechanical properties and susceptibility to environmental degradation.[41,42] However, in the present case, the varying amount of oxygen is more likely to be related to the different thicknesses of the oxide layer, as will be shown below by XPS. Another possibility is surface contamination, but in that case, the variability of oxygen content would be smaller.

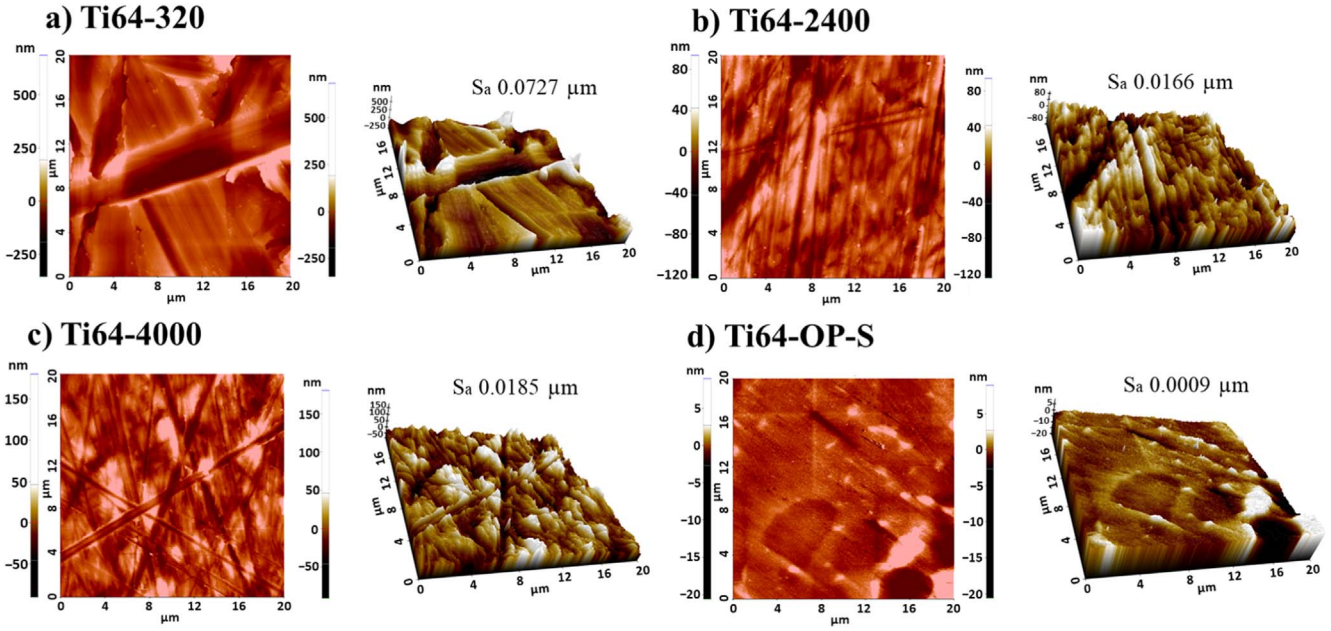

Figure 2. The top-view and 3D profiles of AFM images recorded on a 20 µm × 20 µm area on differently metallographically prepared Ti-6Al-4V samples. S_a values are given in the figure.

The SEM/EDXS analysis of diamond-polished Ti64-DP-L and chemo-mechanically polished Ti64-OP-S samples was conducted at higher magnification and using back-scattered images to address the chemical differences at the surface in more detail, including the absence of oxygen for the Ti64-OP-S sample (Fig. 4 and Table III). Compared to analyses presented in Fig. 3 and Table II, much larger variations in composition were observed. However, even using the CBS detector (BSE mode), differences in individual phases were clearly distinguished only for Ti64-OP-S samples (Figs. 4c, 4d) but much less for diamond-polished (Figs. 4a, 4b) and ground (not shown) samples. Due to the use of a CBS detector, the compositions of individual phases differ in colour, making them brighter for the phases containing lighter elements.

First, we consider diamond-polished samples (Figs. 4a, 4b and Table III). The average composition (site 1) consisted of 83.6% Ti, 5.6% Al and 3.4% V. However, at sites 1a and 1b, the contents of Ti, Al and V change depending on whether α-matrix (site 1b) or β-phase (site 1a) was considered. No V was present in the α-matrix, whereas the β-phase was rich in V (11.6%). Oxygen content ranged from 5.3 to 7.4% by weight; no carbon or iron was present.

Different phases were noted within the microstructure of the Ti64-OP-S sample (Figs. 4c, 4d and Table III). The average composition (site 2) consisted of 89.7% Ti, 6.0% Al and 4.3% V. Higher magnification (Fig. 4d) revealed α-matrix (site 2 d) containing only Ti and Al, and β-phase with grains 2a and 2b rich in vanadium (ca. 18%). β-phase with grain 2c contains less vanadium than sites 2a and 2b. The striking difference was the content of oxygen, which was not detected in the Ti64-OP-S sample but only for ground (not shown) and diamond-polished samples, thus confirming the result from Fig. 3. We assumed that the differences in O content for differently metallographically prepared samples reflect the differences in the thickness of the Ti oxide layer, which is in the nanometric range.[13] When using EXDS analysis at 10 kV accelerating voltage, the analysis depth is almost 1 micrometre. Hence, EXDS analysis performed at 10 kV is insufficiently sensitive to study the difference in nanometric surface layers. Since no observation in the literature was reported on this issue, XPS was used to address this matter further. The XPS analysis has an analysing depth of up to 10 nm and is thus more suitable. Furthermore, depth profiling was used to account for the layers' depth.

XPS analysis was performed for two representative samples—ground Ti64-4000 and chemo-mechanically polished Ti64-OP-S. The survey spectra (results not shown) showed a similar general composition with Ti and O as the principal elements and a high concentration of adventitious carbon. Al was almost non-detectable for Ti64-4000, but it was detected for Ti64-OP-S. Vanadium was not detected on either sample. Some other elements were also detected, like nitrogen, phosphorus, zinc and calcium, which are impurities or contaminants from the metallographic preparation process.

Further, high-energy resolution spectra of Ti 2p, Al 2p, O 1 s and V 2p were inspected for the speciation of the elements. Spectra recorded at the surface and 40 nm depth are presented in Figs. 5 and 6.

First, the surface composition of Ti64-4000 was considered (Fig. 5). The Ti $2p_{3/2}$ and $2p_{1/2}$ peaks were centred at 458.4 eV and 464.2 eV, respectively, corresponding to TiO_2.[13] The O 1 s spectrum was centred at 529.9 eV (corresponding to O^{2-} species) with another peak at 531.4 eV (corresponding to OH^- species), aligned with the formation of Ti hydrated oxide. Al 2p and V 2p signals were very low, indicating that, after grinding, the upper surface contained predominantly Ti oxide.

The Ti 2p and O 1 s spectra recorded at the surface of Ti64-OP-S are presented in Fig. 6. The O 1 s spectrum showed no particular difference compared to those of Ti64-4000 (Fig. 5); it was also centred at 532.0 eV, with the shoulder at 531.3 eV, aligned with the formation of Ti hydrated oxide. In the Ti 2p spectrum, in addition to the peaks corresponding to TiO_2, the peaks related to Ti metal were present with the Ti $2p_{3/2}$ peak centred at 453.7 eV. This finding indicated that the Ti oxide is sufficiently thin to detect the underlying Ti metal (considering the analysis depth of a few nanometres). Another possibility would be that the Ti oxide did not cover the whole uppermost surface but contained non-oxidised parts exposing Ti metal. However, even if this is the case, exposed metal would be self-passivated, but the oxide layer would be thinner at these spots. The Al 2p spectrum showed a small, indistinctive peak at ca. 74 eV (Fig. 6b), corresponding to Al_2O_3 [13], which was hardly visible for the Ti64-4000 sample. No V was present at the surface. Therefore, based on the XPS analysis of the sample outermost surface, it can be stated that both samples are composed predominantly of a TiO_2 layer, which is thinner for the Ti64-OP-S sample.

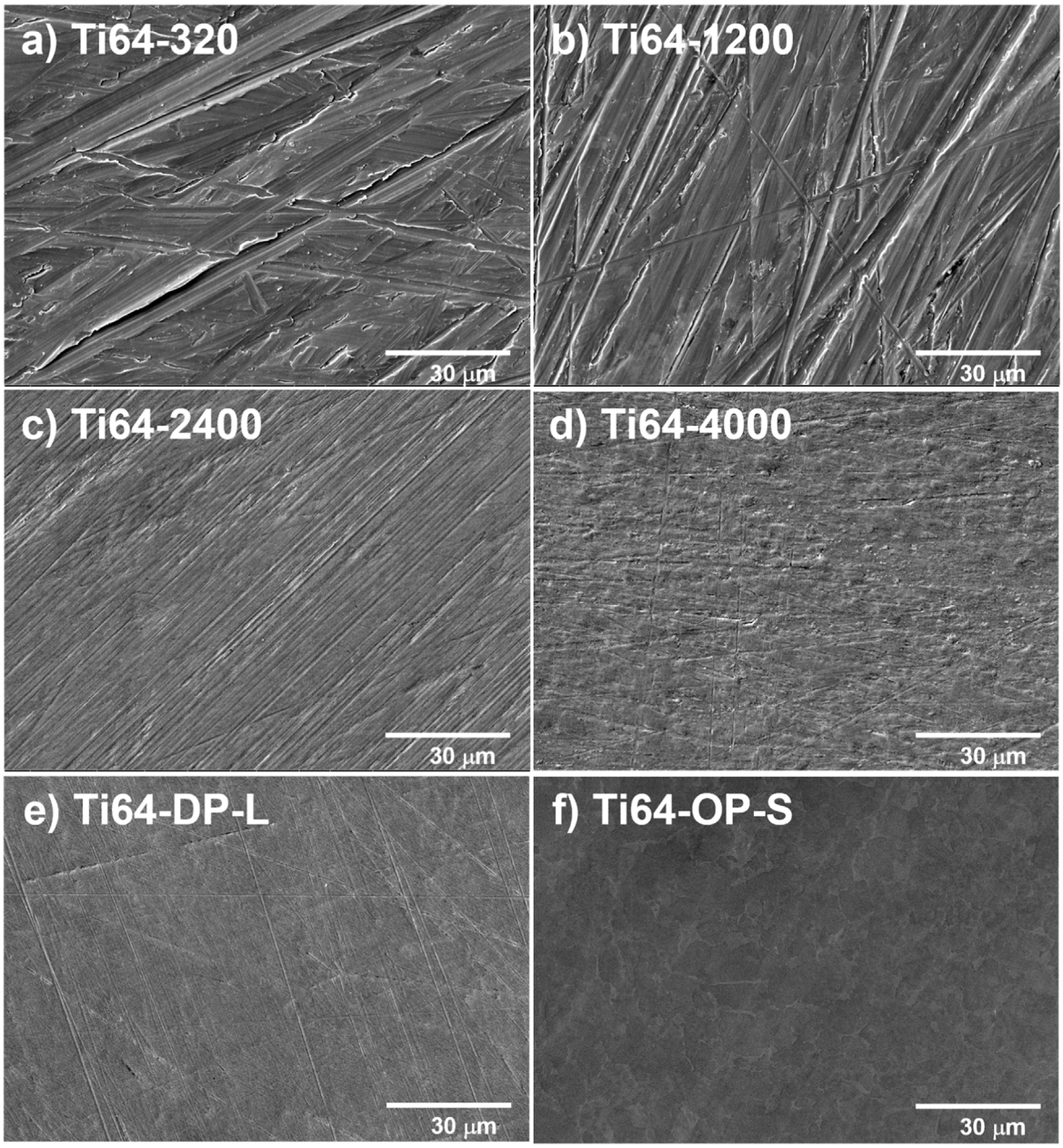

Figure 3. SEM secondary electron image microphotographs recorded at 10 kV showing the morphology of Ti-6Al-4V alloy after grinding with different SiC grit paper (a) #320-grit, (b) #1200-grit, (c) #2400-grit, (d) #4000-grit, (e) diamond polished (DP-L) and (f) chemo-mechanically polished (OP-S) at a magnification of 1000 ×. EDXS analysis was made on the entire area shown in particular image. The results are presented in Table II.

Table II. The chemical composition of Ti-6Al-4V samples depending on the metallographic preparation. The composition given in weight percentage (wt%) was determined by EDXS analysis performed on SEM images in Fig. 3.

Composition (wt%)	Metallographic preparation					
	Ti64-320	Ti64-1200	Ti64-2400	Ti64-4000	Ti64-DP-L	Ti64-OP-S
Ti	86.8	87.9	76.8	81.7	83.6	89.7
Al	5.9	5.9	5.1	5.9	5.6	6.0
V	3.6	3.7	4.5	4.1	3.4	4.3
O	3.7	2.5	12.1	6.9	7.4	0.0
C	0.0	0.0	1.5	1.4	0.0	0.0
Total/wt%	100.0	100.0	100.0	100.0	100.0	100.0

Depth profiles of Ti64-4000 and Ti64-OP-S samples showing the dependence of the chemical composition as a function of sputtering time are presented in Figs. 7a, 7b. Only the main elements, Ti, O, Al, V and C, are presented in the profiles. Starting from the surface of the Ti64-4000 sample, where Ti, O and C were the principal constituents, the Ti signal started to increase, and that of O decreased as the sputtering progressed (Fig. 7a). The adventitious carbon signal decreased immediately below the surface. At the same time, Al and V gradually appeared as the oxide layer progressively sputtered away. Vanadium cannot be regarded as a part of the oxide layer. However, Al 2p spectra presented at different depths show that the peak related to Al_2O_3 (at 74 eV) is present below the surface and only at a certain depth is shifted to the range of Al metal (Fig. S2). This indicates that Al_2O_3 is a part of the surface oxide. For Ti64-4000, the curves for Ti and O intersected at 9 min (9 nm) and those of Ti64-OP-S at about 3 min (3 nm). Accounting for the common rule that the oxide

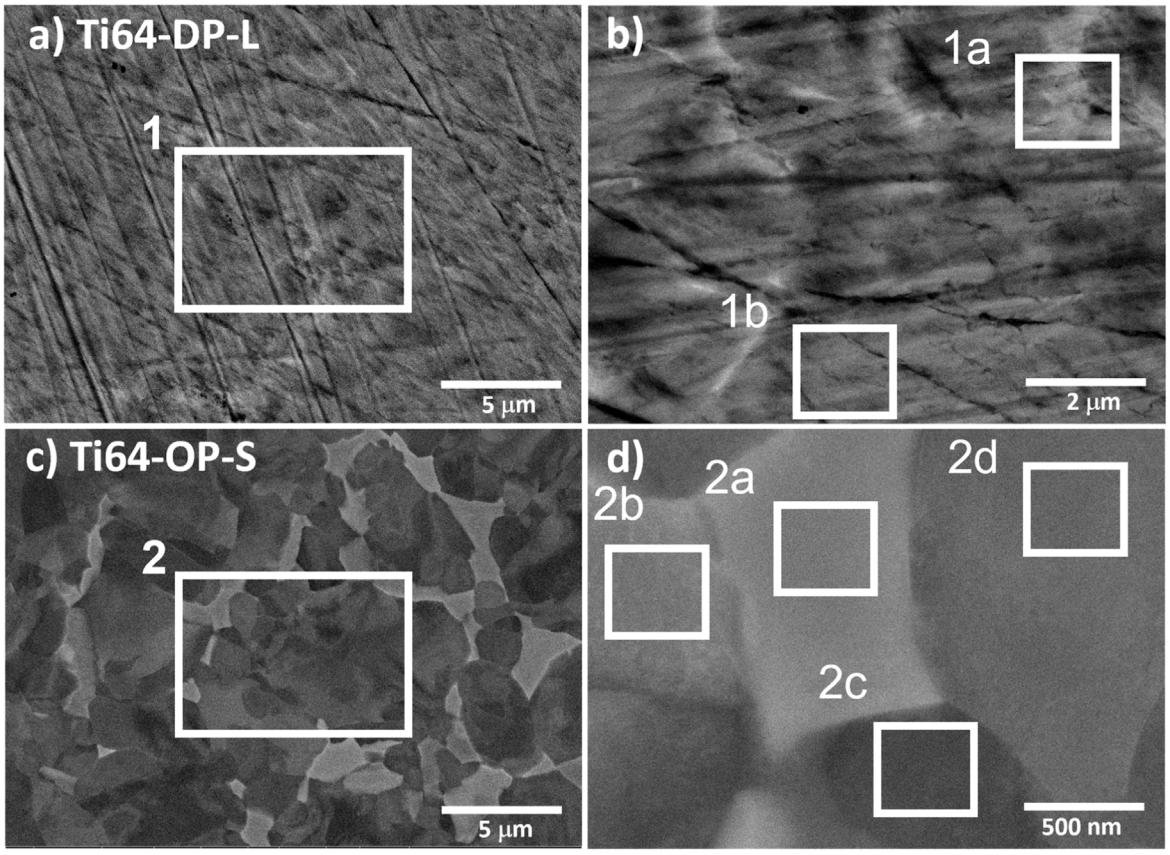

Figure 4. SEM back-scattered electron microphotographs recorded at 10 kV showing the morphology of Ti-6Al-4V alloy after (a,b) diamond polishing (DP-L) at a magnification of (a) 5,000 × and (b) 12,000 × and (c), (d) chemo-mechanical polishing (OP-S) at a magnification of a (c) 5,000 × and (d) 50,000×. EDXS analysis conducted at enumerated sites is presented in Table III.

Table III. The chemical composition of Ti-6Al-4V prepared by diamond polishing (DP-L, sites 1 and 1a,b) and chemo-mechanical polishing (OP-S, sites 2 and 2 a–d) determined by EDXS analysis performed on denoted sites in SEM images in Fig. 4.

	Metallographic preparation							
	Diamond-polished sample			Chemo-mechanically-polished sample				
Composition (wt%)	1	1a	1b	2	2a	2b	2c	2 d
Ti	83.6	79.2	88.6	89.7	76.3	76.2	88.3	92.2
Al	5.6	3.9	5.9	6.0	2.9	3.0	6.2	6.4
V	3.4	11.6	0.0	4.3	17.5	18.6	4.2	0.0
O	7.4	5.3	5.5	0.0	0.0	0.0	0.0	0.0
C	0.0	0.0	0.0	0.0	0.0	0.0	1.3	1.4
Fe	0.0	0.0	0.0	0.0	3.3	2.2	0.0	0.0
Total/wt%	100.0	100.0	100.0	100.0	100.0	100.0	100.0	100.0

thickness related to the time at which oxygen concentration drops to half from that at the surface, the deduced thickness of the layers would be larger, i.e., around 15 nm and 4 nm, respectively. The Linear Least Square (LLS) fitting tool for processing XPS depth profile data allows the decomposing of XPS spectra recorded during the profile into metal and oxide components and then displaying the curves as a function of depth (Figs. 7c, 7d). In this way, a more accurate determination of oxide thickness is achieved than from conventional depth profiles, which include various artefacts of sputtering leading to prolongation of the oxygen signal into the layer depth, not necessarily reflecting the layer thickness. The intersection between Ti 2p peaks for oxide and metal located at 5.5 nm for Ti64-4000 (Fig. 7c), i.e. smaller than determined from the intersection or based on a 50% oxygen content rule but accounting for a more realistic situation.

The Ti 2p and Al 2p spectra as a function of sputtering time throughout the profile are presented in Fig. S2. In Figs. 5 and 6, only spectra recorded at a depth of 40 nm are compared to those at the surface. The position of the Ti $2p_{3/2}$ peak gradually shifted from 453.7 eV, corresponding to TiO_2, to 456.8 eV, corresponding to Ti metal. At the same time, the Al 2p peak appeared immediately below the surface, indicating that Al was present within the oxide but buried below the outermost Ti oxide layer. The Al 2p peak at ca. 74 eV confirms that Al was oxidised and present as Al_2O_3 oxide, as shown previously.[13] As the sputtering proceeded toward the layer depth and interface with the underlying substrate, the centre of the

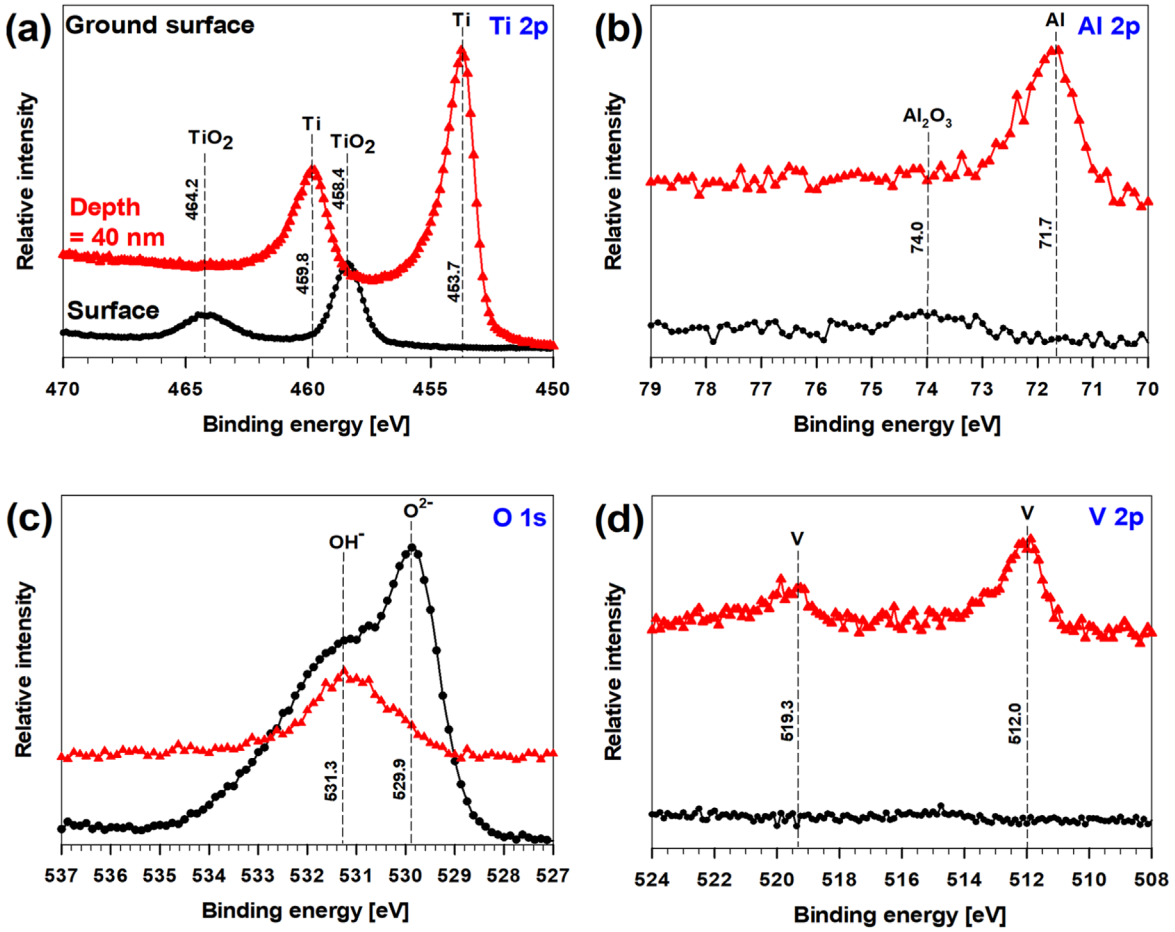

Figure 5. XPS Ti 2p, Al 2p, O 1 s and V 2p spectra recorded at the surface and a depth of 40 nm of the Ti-6Al-4V sample after grinding with SiC papers up to 4000 grit (Ti64-4000).

Al 2p peak shifted to the region of Al metal, i.e. 71.7 eV. Vanadium was not detected within the surface layer, which is consistent with previous work.[13] The vanadium signal appeared at a depth of ca. 5 nm, increasing its intensity towards the inner interface. At a depth of 40 nm, Ti $2p_{3/2}$ and $2p_{1/2}$ peaks were centred at 453.7 eV and 459.8 eV, aligned with Ti metal. The Al 2p peak was positioned at 71.7 eV, corresponding to the Al metal, and the V $2p_{3/2}$ at 512 eV related to the V metal.

Like the Ti64-4000 sample, Ti, O and C were the principal constituents at the surface of the Ti64-OP-S sample (Fig. 7b). In contrast to the Ti64-4000, whose oxide layer was 5.5 nm thick, the layer formed in Ti64-OP-S sample was only 2.7 nm, as determined by LLS fitting (Fig. 7d). These data show that the Ti oxide layer thickness spontaneously formed on the ground surface is doubled that on the Ti64-OP-S surface.

Literature data on the surface composition of the ground and polished Ti or Ti-alloy indicates some changes caused by the metallographic preparation, but no systematic comparison could be found, as in this study. Ozdemir et al. reported that after chemo-mechanical polishing by alumina nanoparticles and H_2O_2 at pH 4, a protective TiO_2 layer was formed on Ti, as shown by XPS.[38] However, although the peak related to Ti metal was evident in the XPS spectra, similar to the present study (Fig. 6), its appearance was not specifically commented. In another study, the effect of chemo-mechanical polishing was commented on only through O 1 s spectra but not Ti 2p spectra.[40] The O^{2-}, OH^- and H_2O species ratio changed from the layer's interior towards the outermost surface.[40] In contrast, Zhang et al. observed by XPS that the outermost surface of the Ti-6Al-4V sample chemo-mechanically polished with silica nanoparticles, 40 wt% H_2O_2 and malic acid contained predominantly TiO_2, but also Ti metal, and Al_2O_3 and V_2O_5.[39] These features were ascribed to a prominent oxidation reaction caused by H_2O_2, resulting in the formation of oxides. All elements were in metal states at 10 nm below the surface.[39]

The formation of a thinner oxide layer is related to the nature of the chemo-mechanical polishing process, where a continuous action of SiO_2 abrades the surface, and H_2O_2 oxidises it. The concentration of H_2O_2 affects the rate of removal of the surface oxide due to the chemical action of H_2O_2, being a strong oxidant in acidic and alkaline media.[36–40] During polishing, the surface oxide layer is removed by the action of silica nanoparticles, thus exposing the underlying Ti substrate. Due to the action of H_2O_2, the substrate exposed to the slurry can be oxidised according to:

$$Ti + 2H_2O_2 \rightarrow TiO_2 + 2H_2O \quad [1]$$

It is well known that even without the action of H_2O_2, Ti spontaneously forms a passive oxide layer upon exposure to air.[13] The following reaction can be generalised:[43]

$$Ti + nH_2O \rightarrow Ti(OH)_n + n/2\ H_2 \quad [2]$$

During CMP, therefore, the removal of the oxide layer and its reforming proceed simultaneously, resulting in a mirror-polished surface. The prevalence of one or another process depends on the rate-determining step. At low H_2O_2 concentrations, the reformation of TiO_2 is slower, and the oxide layer cannot form again due to the abrasive action of silica, resulting in the exposure of the underlying metal.[36] At higher oxidant concentrations, the oxide layer can reform sufficiently fast. In the present study, a relatively high concentration of 10 v/v% H_2O_2 was used, and it seems that the rate of layer

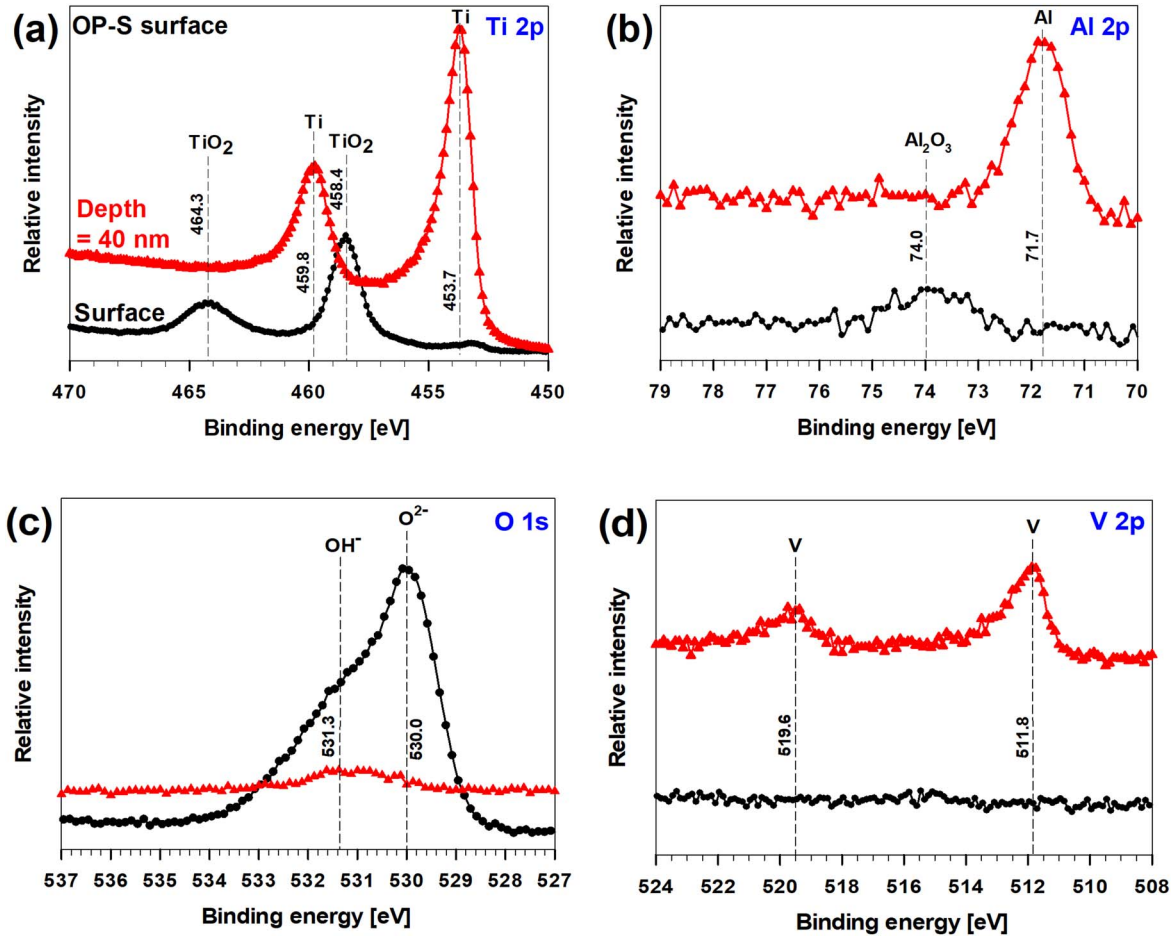

Figure 6. XPS Ti 2p, Al 2p, O 1 s and V 2p spectra recorded at the surface and a depth of 40 nm of the Ti-6Al-4V sample after chemo-mechanical polishing (Ti64-OP-S).

reforming is comparable to that of layer removal, although some spots may remain non-oxidised. Those spots would be immediately self-passivated, but the layer thickness would be smaller than in the absence of H_2O_2, as confirmed experimentally (Fig. 7).

Electrochemical measurements of the Ti-6Al-4V samples subject to different metallographic preparations.—Electrochemical measurements were performed in two simulated physiological solutions relevant to biomedical applications 0.9 wt% NaCl and artificial saliva. Before the EIS measurements, the samples were stabilised at the open circuit potential for 1.5 h. OCP values ranged between −0.30 V and −0.37 V, with no particular trend between the differently metalographically prepared Ti-6Al-4V samples (Table SI). Following the stabilisation time, EIS spectra were conducted. Nyquist plots of imaginary impedance component (Z″) vs real impedance component (Z′) (Fig. 8) and Bode plots of magnitude of impedance |Z| and phase angle (Θ) vs frequency (*f*) (Fig. 9) were measured at OCP for differently prepared Ti-6Al-4V samples. All Ti-6Al-4V samples exhibited Nyquist plots with only one capacitor arc with a very large radius. The latter depended on the metallographic preparation and changed from a half-semicircle for the roughest surface of Ti64-320 to an initial part of a semicircle for smoother samples such as Ti64-OP-S. These plots confirm a near-capacitive response in NaCl and artificial saliva solutions. From the Bode plots of magnitude of impedance, it was hard to distinguish the differences between the samples; in all cases, a protective layer was formed at the surface, as evidenced by a linear dependence of |Z| vs frequency down to 0.01 Hz and quite broad frequency region of constant phase angle values. However, some differences were observed, with phase angles deteriorating at frequencies below 0.1 Hz. EIS data were fitted to quantify the differences in electrochemical characteristics. A simple electrical equivalent circuit (EEC) was used consisting of an *R*–*C* parallel combination in series with an ohmic resistance given by the electrolyte resistance (R_s) (Fig. 9a) representing a passive titanium oxide film. Thus, the impedance response relates to the overall polarisation resistance (R_p), including the oxide and possible corrosion products in the pores and metal interface. Since the slope of the log|*Z*| vs log(*f*) plot is not −1 and the phase angle does not reach −90°, the electrode impedance is best described by a constant-phase element (CPE).[24,44]

The fitting results are presented in Tables IV and V. Let us first consider the measurements in 0.9 wt% NaCl. χ^2 values were less than $3{\cdot}10^{-2}$ (Table IV), and the errors in R_p ranged between 1.3 and 9.2%. Polarisation resistance values were between 818 kΩ·cm^2 for the Ti64-DP-L sample and over 8 MΩ·cm^2 for the Ti64-OP-S, indicating that barrier layers with strong protective properties were formed in the latter case. Some differences between the samples are noted. Considering only ground samples, the R_p increased from Ti64-320 to Ti64-1200, reaching a maximum of 2633 kΩ·cm^2, i.e. about three-fold. R_p then decreased over Ti64-4000 to Ti64-DP-L, reaching 818 kΩ·cm^2. The values of CPE were similar for all the samples. The values of *n*, i.e., the slope of the log |Z| vs log *f*, were between 0.904 and 0.938, again confirming a high capacitive character of the passive layers formed upon immersion of Ti-alloy in NaCl solution. As evident in Fig. 9a, the Θ values scattered, reaching a maximum of −71° for the Ti64-1200 sample among ground samples and increasing to –81° for the polished sample. The changes in Θ at low frequency (10 mHz) may be related to the presence of pores and defects in the layer formed by rough grinding. The polished sample, in contrast, exhibited the highest Θ, showing the smallest deviation from the Θ of an ideal capacitor (−90°).

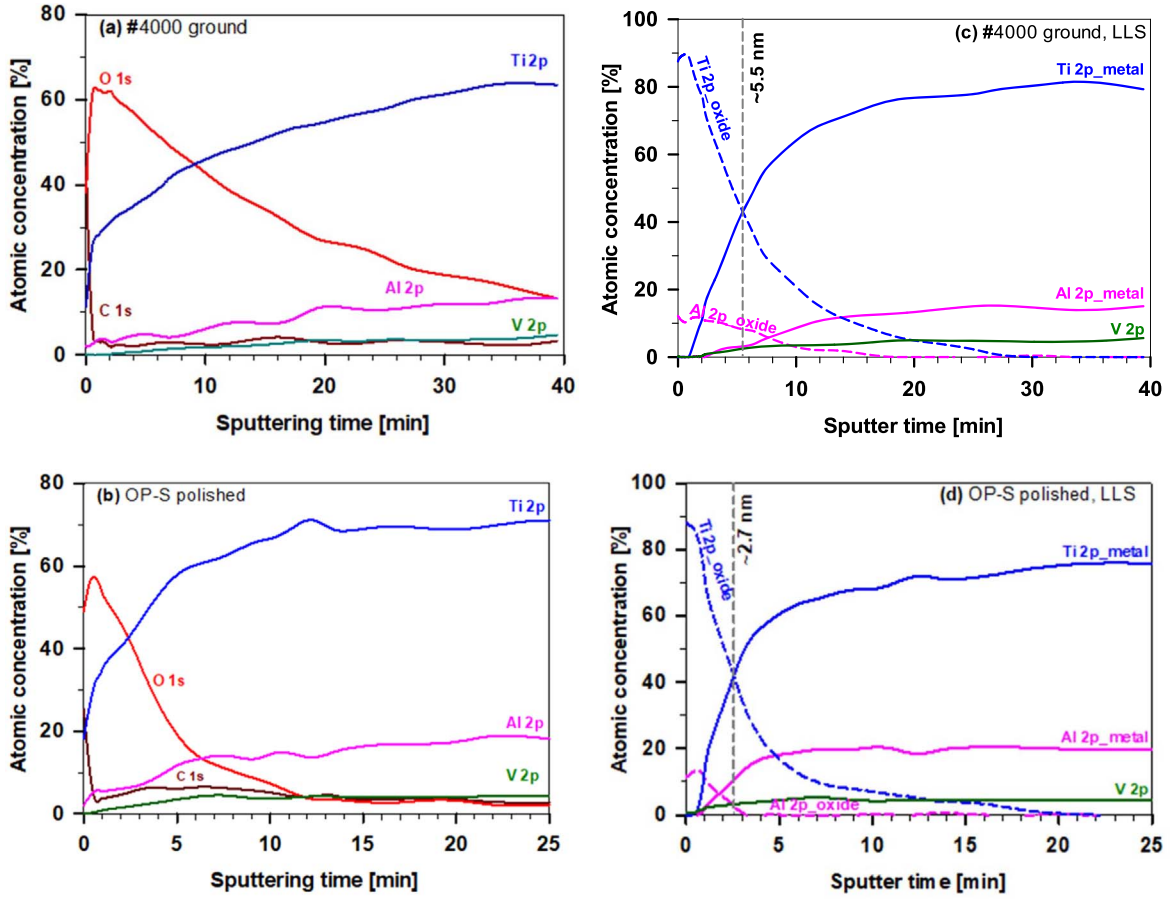

Figure 7. XPS depth profiles of Ti 2p, Al 2p, O 1 s, V 2p and C 1 s recorded at the surface of Ti-6Al-4V samples after (a), (c) grinding with SiC papers up to 4000 grit (Ti64-4000) and (b), (d) after chemo-mechanical polishing (Ti64-OP-S). Sputtering rate was 1.0 nm min^{-1}. Depth profiles (c) and (d) were obtained using the LLS fitting tool to account for a more accurate determination of oxide thickness.

In artificial saliva, the general shapes of the curves were similar to.9% NaCl solution (Fig. 9b, Table V). The fitting revealed several differences. χ^2 values were less than $1.3{\cdot}10^{-2}$, and the errors in R_p ranged between 0.2 and 4.6%. The R_p values for all the samples except Ti64-320 were larger, indicating that the passive layers formed in artificial saliva expressed somewhat more protective properties than those in NaCl solution, possibly due to phosphate added to saliva. However, the overall behaviour of the Ti-6Al-4V samples in both solutions was similar, showing a strong capacitive character. The polished Ti64-OP-S samples were superior to the best-performing ground samples, showing approximately threefold R_p values and higher Θ.

The EIS results obtained at the OCP suggest that the metallographic preparation affects the electrochemical response of Ti-6Al-4V in simulated physiological solutions. Distinctive differences were observed when measuring electrochemical properties in the broad potential region. Following the EIS measurements, potentiodynamic polarisation curves of Ti-6Al-4V samples with six different surface finishes (ground up to #4000 SiC, diamond-polished and silica-polished) were measured in 0.9 wt% NaCl and artificial saliva (Fig. 10). To avoid completely removing the spontaneously formed oxide layer, the cathodic branch was initiated only at −0.1 V vs OCP. Therefore, we were focused mainly on the anodic polarisation behaviour. The j_{corr} value was determined as the intersection of the tangent to the anodic branch of the PDP curve and the line through the E_{corr}. Electrochemical parameters determined from experimental PDP curves are presented graphically in Fig. 11. Data in tabular form are given in Table SI.

The PDP curves are typical for Ti-alloys in simulated physiological solutions with two distinguished regions.[13,24–26] At potentials above E_{corr}, current density increased in the Tafel region and reached the first current density plateau at ca. 0.1 V (the E_{p1}). This plateau extends to ca. 2.5 V. As shown previously by XPS, this region is characterised by forming predominantly TiO_2 but also Ti-suboxides (TiO and Ti_2O_3).[13] Aluminium oxide is also partially incorporated into the surface layer. The shape and extension of the first plateau appeared similar for all investigated samples, showing current density values within the same order of magnitude, i.e. 5 − 8 μA cm^{-2}. It indicates passive behaviour for all samples, suggesting the spontaneous formation and thickening of a passive film on the surface. The first plateau ended at the $E_{p1'}$ at ca. 2.5 V. At more positive potentials, the current density increased, forming a peak between 2.5 and 4 V. The peak was highest for the Ti64-OP-S sample and lowest for the Ti64–2400 and Ti64-4000 samples. According to previous XPS analysis,[13] above the current density peak, further oxide formation occurred; the Ti suboxide cannot be observed at the surface anymore, which is composed entirely of TiO_2. In this region, the content of Al_2O_3 in the layer increased.[13] The current density peak feature on titanium was ascribed to the change in the film growth such that the relatively rapid growth of amorphous oxide gives way to low oxide growth, together with gas evolution associated with crystalline oxide in the film.[45] In the range of the current plateau (extending from E_{p2} to $E_{p2'}$), the current density remained independent of potential up to 6 V. However, as discussed in the text below, an abrupt increase in current density was observed for Ti64-320 and Ti64-1200 samples, indicating localised passive film breakdown. Metikoš-Huković et al. reported that the oxide layer formed on Ti-6Al-4V may suffer from localised breakdown and pitting corrosion in SBF due to the presence of insufficient annihilation of anion vacancies when alloying TiO_2 with V and thus being susceptible to breakdown.[46]

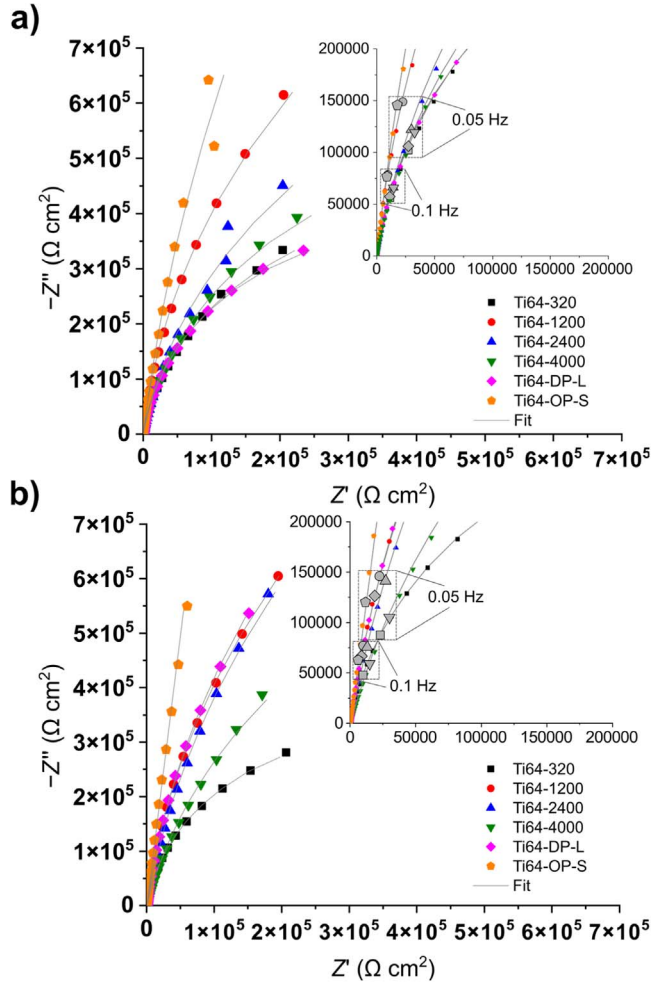

Figure 8. Nyquist plots recorded for differently metallographically prepared Ti-6Al-4V samples at OCP in (a) 0.9 wt% NaCl solution and (b) artificial saliva solution at 37 °C after 1.5 h of immersion. Experimental data are presented by symbols and fitted results by lines. Insets show the magnified initial parts of the curves with denoted values at 0.05 Hz and 0.1 Hz (enlarged symbols).

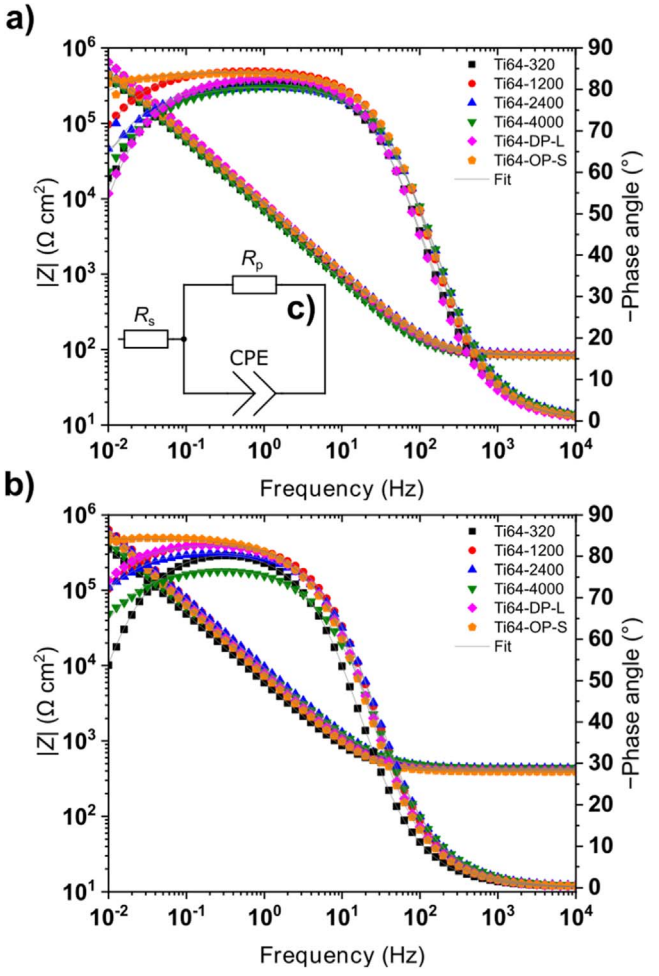

Figure 9. Bode plots of magnitude of impedance and phase angle recorded for differently metallographically prepared Ti-6Al-4V samples at OCP in (a) 0.9 wt% NaCl and (b) artificial saliva solution at 37 °C after 1.5 h of immersion. Experimental data are presented by symbols and fitted results by lines. (c) The electrical equivalent circuit used for fitting.

First, we consider the results in 0.9% NaCl solution in more detail (Figs. 10a and 11, Table SI). E_{corr} values ranged from −0.38 V to −0.34 V with no clear trend depending on the surface roughness (Fig. 11a). In contrast, j_{corr} values show a decreasing trend from 0.043 to 0.014 μA cm^{-2} from the roughest towards the smoothest surface (Fig. 11b). Thus, rougher ground surfaces exhibited a higher corrosion susceptibility than smoother ground surfaces. The diamond and chemo-mechanically polished surfaces exhibited three times smaller j_{corr} than the #320-SiC ground surface. At the first plateau (from E_{p1} to $E_{p1'}$), the current density was quantified at 1 V ($j_{=1V}$). Although all samples showed similar curves (Fig. 10a), the quantification of $j_{=1V}$ showed two trends (Fig. 11c): a decreasing trend for ground samples from rougher to smoother surface (from #320 to #4000 SiC-grit, Fig. 1) with $j_{=1V}$ from 8.3 to 5.6 μm cm^{-2}. However, the trend changed for polished samples, again exhibiting larger current densities. This reversing trend became even more apparent at the second current density plateau from E_{p2} to $E_{p2'}$, with current densities stretching over two orders of magnitude (Fig. 10a). The current density values were quantified at 3.5 V ($j_{=3.5V}$), i.e. roughly at the current peak (Fig. 11d). The $j_{=3.5V}$ values, which were three orders of magnitude larger than $j_{=1V}$, decreased from 286 μm cm^{-2} for Ti64-320 to 15 μm cm^{-2} for Ti64-4000, where a minimum was reached. For the Ti64-OP-S sample, $j_{=3.5V}$ increased enormously to over 1 mA cm^{-2} (Fig. 11d). At potentials above the current peak, > 4 V (Fig. 10), the differences in current densities of different samples became much smaller than in the range of the current peak leading to a relative equalisation between the samples (within one decade of magnitude). This behaviour leads to the conclusion that the initially thinnest layer on Ti64-OP-S (Fig. 7) results in the highest current density peak related to the oxide thickening; once the maximum oxide thickness was reached, the current density declined and formed a plateau as for other samples.

Notably, for samples with the roughest surface finish (Ti64-320 and Ti64-1200), the passivity breakdown occurred at 4.6 V and 5.7 V, respectively (Fig. 10a). For all other smoother surface samples, no passive film breakdown was detected up to 6 V. Passivity window (ΔE_p) was defined as the region extending from the onset of passivation (point of transition from active to first passive current density plateau, E_{p1}) to the onset of the second current density plateau $E_{p1'}$. The widest ΔE_p was registered for the Ti64-4000 ($\Delta E_p = 2.35$ V) and Ti64-2400 samples ($\Delta E_p = 2.45$ V), while the narrowest was for the Ti64-OP-S sample ($\Delta E_p = 1.80$ V). The Ti64-320, Ti64–1200, and Ti-DP-L exhibited ΔE_p of 2.0 V, 1.9 V and 2.2 V, respectively (Table SI).

Similar current-voltage curves were recorded in artificial saliva solution as in 0.9 wt% NaCl (Fig. 10b). However, some differences were distinguished. E_{corr} values were more negative than those for the NaCl solution. For ground samples, E_{corr} shifted more negatively, ranging from −0.38 V to −0.46 V (Fig. 11a); for the two polished samples, the E_{corr} shifted positively again. The decreasing trend of j_{corr} from the roughest towards the smoothest surface, was

Table IV. Values of fitted parameters of EIS measurements in 0.9% NaCl presented in Figs. 8a and 9a using EEC in Fig. 9a. χ_2 values denote the goodness of the fit.

Sample	R_s/Ω·cm^2	R_p/kΩ·cm^2	CPE (Y_0) ·10^{-5}/(μΩ^{-1} s^n cm^{-2})	n	χ^2	Phase angle at 10 mHz
Ti64-320	83	893	2.67	0.918	0.0108	−58
Ti64-1200	85	2633	1.97	0.945	0.0040	−71
Ti64-2400	86	1677	2.21	0.904	0.0306	−65
Ti64-4000	82	1167	2.26	0.906	0.0237	−60
Ti64-DP-L	83	818	2.61	0.932	0.0088	−55
Ti64-OP-S	85	8092	2.00	0.938	0.0102	−81

also observed (Fig. 11b). Similarly, $j_{=1V}$ and $j_{=3.5V}$ values followed similar trends as in the NaCl solution, with somewhat smaller current density values (Figs. 11c, 11d) and broader ΔE_p (Table SI). The widest ΔE_p was registered for the Ti64-4000 sample ($\Delta E_p = 3.0$ V) and Ti64–2400 sample ($\Delta E_p = 2.8$ V), while the narrowest passivity window was for the Ti64-OP-S sample ($\Delta E_p = 2.0$ V).

All samples showed a passive behaviour up to approximately 2.5 V to 3 V vs Ag/AgCl, suggesting the spontaneous formation of a passive film on the surface of Ti-6Al4V in artificial saliva, as characteristic of Ti-based alloys.[47] The increase of current density at potentials higher than 2.5 V is highest for Ti64-OP-S and lowest for Ti64-4000 sample. No passive film breakdown was detected during the polarisation tests in the artificial saliva solution compared to 0.9 wt% NaCl solution. Such observation suggests better stability of passive film formed in artificial saliva, as noted previously for CoCrMo alloy.[48]

Elaboration on the effect of metallographic preparation on surface properties and electrochemical measurements.—The EIS and PDP results for differently metallographically prepared samples were generally very similar but with some distinctive differences. A closer inspection reveals that in EIS spectra, the metallographic preparation affected R_p and Θ. For ground samples in NaCl solution, R_p values determined from EIS spectra spanned within a threefold range, with the samples ground using 1200, 2400 and 4000 grits showing larger values than Ti64-320 and Ti64-DP-L samples. The Ti64-OP-S sample showed tenfold larger values than the latter two. Similarly, for Ti64-320 and Ti64-DP-L samples, Θ values were the smallest (<60°), intermediate for Ti64-1200, Ti64-2400 and Ti64-4000 (60°–70°), and >80° for Ti64-OP-S. In artificial saliva, somewhat different R_p and Θ values were obtained than in NaCl solution, but a general trend is similar. Therefore, based on the EIS measurements, it can be concluded that polished samples exhibit superior performance over ground samples.

The PDP curves recorded over a broad potential span revealed further differences among the samples (Fig. 10). Although the shapes of the curves were similar in the Tafel region and first current density plateau, differences were observed: j_{corr}, $j_{=1V}$ and $j_{=3.5V}$ for all ground samples decreased with decreasing roughness. This is generally in line with literature studies.[30–32,34,35] A higher ion release rate was noticed for macro-rough than micro-rough surfaces.[34] However, none of the reported studies have examined the matter systematically for a large span of SiC grits in a broad potential region. The dependence of the j_{corr}, $j_{=1V}$ and $j_{=3.5V}$ on the roughness may be related to the grinding (Figs. 1–4). Spontaneously formed oxide layers on rough surfaces incorporate surface irregularities, possibly pores, kinks and defects, resulting in a higher susceptibility to dissolution at these sites and reflected through the increased current densities. The EIS spectra also reflected this process by reducing phase angle at low frequencies (Fig. 9). The observed increase in current densities, even accompanied by the localised layer breakdown for the two roughest surfaces (Fig. 10a), can be correlated to the recent study by Gai et al.[43] Using in situ monitoring of pH and chloride concentrations inside the pores of different sizes (simulating the crevice environment within Ti-6Al-4V) it was shown that the pore size affects the development of corrosion. With the increase of pore depth, pH decreased, and the concentration of Cl^- increased during immersion for 14 days in phosphate-buffered saline.[43] With the increase in pore depth, the thickness of the protective oxide layer decreased, exposing Ti metal, becoming more susceptible to corrosion due to a smaller supply of oxygen and increased Cl^- concentration, leading to the acidic environment, as in crevice corrosion.[30,43] If we translate these findings to the present results, it can be well accepted that the oxide

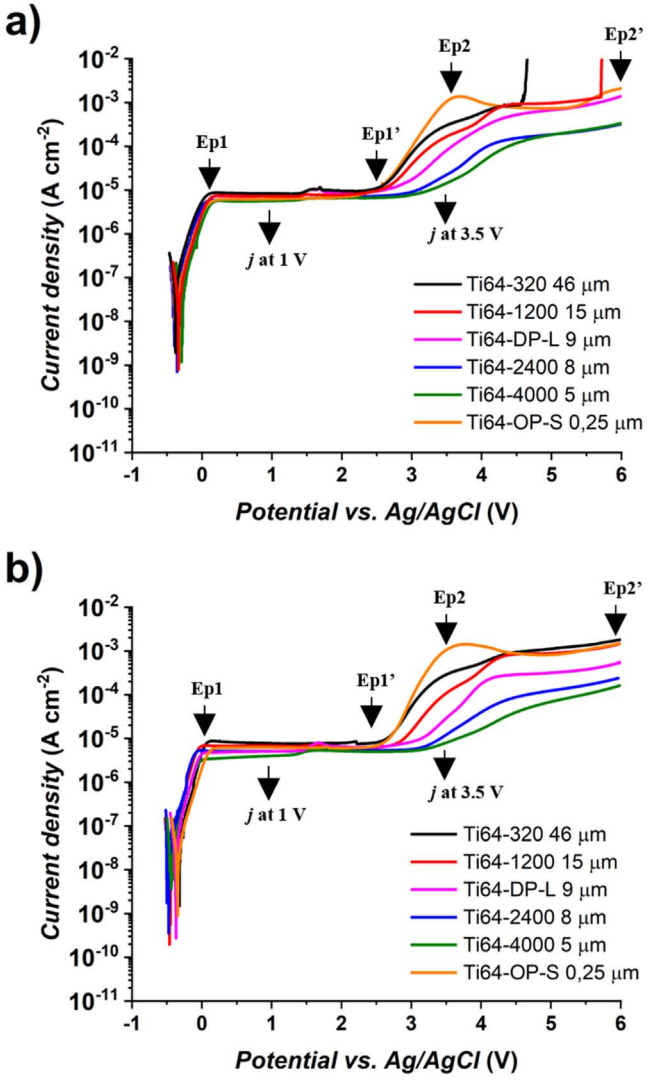

Figure 10. Potentiodynamic polarisation curves of Ti-6Al-4V samples measured in (a) 0.9 wt% NaCl and (b) artificial saliva solution at 37 °C. Samples were prepared using various metallographic preparations, as given in Table I. The gradation of the SiC papers and polishing components are noted in the legend. Electrochemical parameters are presented in Fig. 11.

Table V. Values of fitted parameters of EIS measurements in artificial saliva presented in Figs. 8b and 9b using EEC in Fig. 9a. χ_2 values denote the goodness of the fit.

Sample	R_s/Ω·cm^2	R_p/kΩ·cm^2	CPE (Y_0) ·10^{-5} (μΩ^{-1} s^n cm^{-2})	n	χ^2	Phase angle at 10 mHz
Ti64-320	428	691	3.12	0.922	0.0131	−54
Ti64-1200	418	3073	1.99	0.933	0.0048	−72
Ti64-2400	435	3351	1.97	0.912	0.0121	−72
Ti64-4000	436	1732	2.48	0.872	0.0077	−66
Ti64-DP-L	407	3447	2.29	0.930	0.0070	−74
Ti64-OP-S	393	8798	2.45	0.936	0.0097	−84

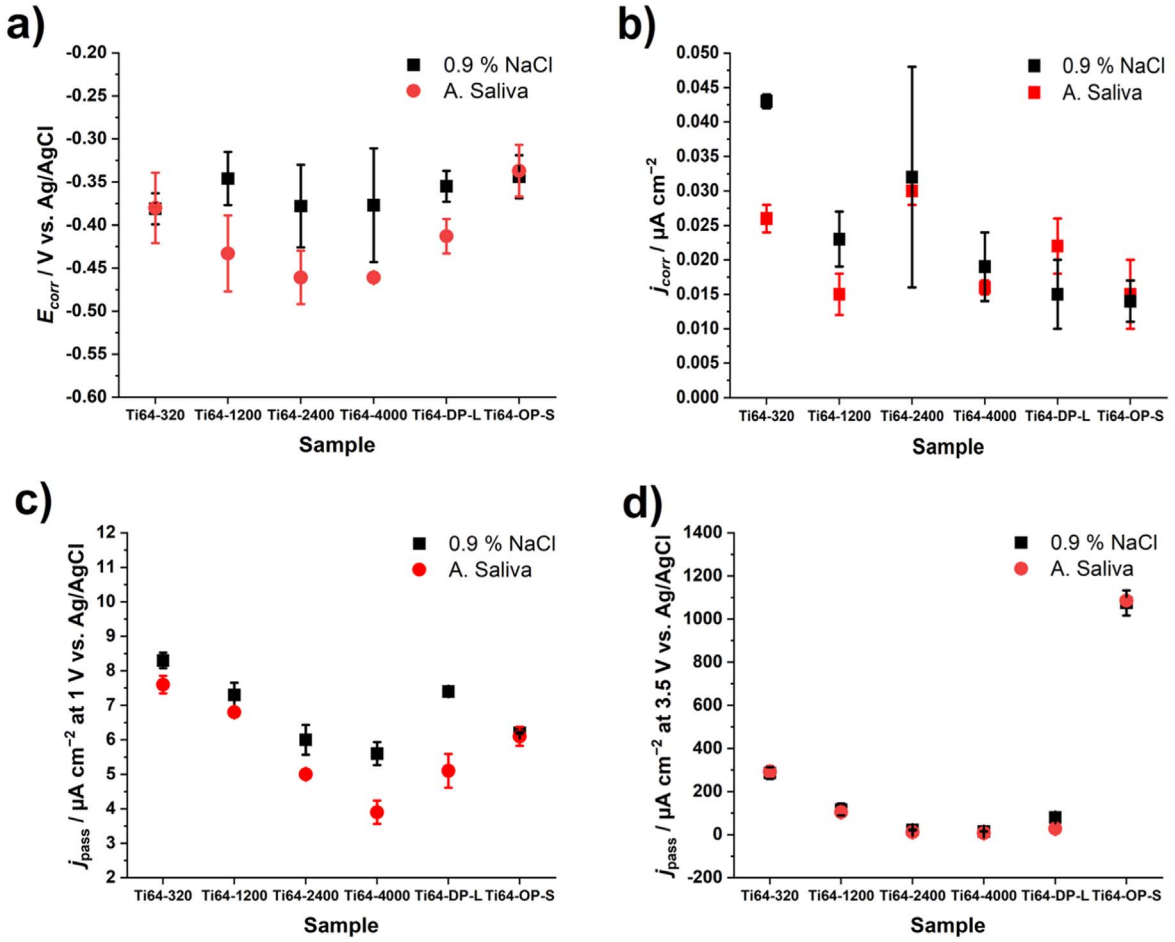

Figure 11. Electrochemical parameters deducted from the PDP curves in Fig. 10: (a) E_{corr}, (b) j_{corr}, (c) j_{pass} at 1 V, and (d) j_{pass} at 3.5 V. Mean values and standard deviations are given.

layer grown on rougher surfaces containing pores or defects leads more readily to increased dissolution.

The reaction (2) proceeds at most of the surface, thickening the oxide layer. However, in the surface defects and/or pores, consumption of oxygen and enrichment of Cl^- leads to the formation of complexes $[TiCl_6]^{2-}$, reaction (4), which can be further transformed by hydrolysis within the pores to TiO_2, reaction (5), and prevent the corrosion of titanium:

$$Ti + 6Cl^- \rightarrow [TiCl_6]^{2-} + 4e^- \quad [4]$$

$$[TiCl_6]^{2-} + 2H_2O \rightarrow TiO_2 + 6Cl^- + 4H^+ \quad [5]$$

Therefore, although the layer is damaged, it can still be repaired unless the surface is too rough, exposing a large portion of underlying metal that cannot be repaired sufficiently to provide passivation and resulting in a breakdown, as noticed in the present study for the roughest ground surfaces.

The roughness is low for the chemo-mechanically polished sample, and its effect on the increased current density is not as likely to provoke dissolution as for the ground samples. Due to the oxidation action of H_2O_2 and dissolution of Ti during polishing, the thickness of the oxide layer on the Ti64-OP-S sample is the smallest compared to the ground samples. However, despite a small thickness, this layer is capable of protecting the underlying metal, supported by the low surface roughness and the absence of surface irregularities. The most significant differences observed in the second current density plateau ($j_{=3.5V}$) may be related to the variations in initial thickness and roughness of the oxide layers on differently metallographically prepared samples. In addition to the variations in roughness and oxide layer thickness, the possibility of Ti peroxy gel formed from Ti metal and hydrogen peroxide, as

suggested,[49,50] cannot be excluded during the CMP procedure, although it has not been identified by the experimental tools used in the present work.

Conclusions

Ti-6Al-4V samples were prepared by grinding, diamond polishing and chemo-mechanical polishing. The metallographic preparation affects the surface topography, morphology and composition of Ti-6Al-4V samples. As expected, mean surface roughness S_a decreased from 0.243 μm to 0.017 μm starting from #320 SiC grinding to chemo-mechanical polishing. The surface morphology changed from deep longitudinal groves when using #320 SiC to shallow grooves for #2400 SiC grinding. A more even topography is obtained for #4000 SiC and diamond polishing. In all cases, the average composition of the surface refers to ca. 6 wt% Al, 4 wt%V and between 2.5 and 12 wt% O. The oxygen concentration detected by EDXS indicates that immediately following grinding or diamond polishing, Ti-6Al-4V surface is spontaneously oxidised and covered by a protective layer of predominantly TiO_2.

A distinctive microstructure of the Ti6Al-4V alloy with α and β phases cannot be distinguished using secondary or back-scattered electrons SEM images on the ground and diamond-polished surfaces but using EDXS analysis at different spots at the surface, α and β phases can be identified. Chemo-mechanical polishing, however, produces α and β phases visible by SEM imaging due to the combined action of hydrogen peroxide as an oxidant agent and silica as an abrasive agent. When inspected by EDXS at a high voltage, the CMP surface contains only Ti, Al and V without any O. XPS explained the differences in oxygen content. Due to an almost micrometre-sized analysis depth of EDXS, it is unsuitable for inspecting thin oxide layers. In contrast, XPS results showed that ground surfaces are covered by a TiO_2 layer whose thickness is doubled compared to that of the Ti64-OP-S surface (5.5 nm and 2.7 nm, respectively). In addition to TiO_2, the oxide layer spontaneously formed on the Ti-6Al-4V contains a small content of Al_2O_3, which is detected below the surface after a few seconds of sputtering Vanadium was not detected within the surface layer.

The metallographic preparation largely affects the corrosion behaviour of Ti-6Al-4V alloy in 0.9 wt% NaCl and artificial saliva solutions. Although the Ti-6Al-4V samples show passive behaviour in simulated physiological solutions, some differences in the stability of the layers and their susceptibility to dissolution depending on the metallographic preparation were observed. At the open circuit potential, polarisation resistance increased with decreasing roughness, as shown by EIS. The chemo-mechanically polished Ti-6Al-4 samples showed superior corrosion resistance over ground samples. Upon potentiodynamic polarisation, further differences appear between ground and chemo-mechanically polished samples. The ground samples follow the trend of decreasing current density with decreasing roughness, which is related to diminishing pores and defects in the layer, thus making it less prone to dissolution in a chloride-containing medium. The Ti64-OP-S sample shows the highest current density at high positive potentials (>3 V). This behaviour is observed in both simulated physiological solutions and explained by the oxidation of a thinner TiO_2 layer on the Ti64-OP-sample than on ground samples due to the oxidative action of H_2O_2 used for chemo-mechanical polishing and constant removal by silica.

This study shows that differences in interpreting the electrochemical response of Ti-6Al-4V and probably other Ti alloys in simulated physiological solutions largely depend on the metallographic preparations. This issue has not been systematically addressed in the literature and may have caused discrepancies between the published results.

Acknowledgments

The authors acknowledge the Slovenian Research and Innovation Agency (ARIS) for the funding of the project »Antibacterial alloys: Development by additive 3D manufacturing, characterisation and clinical applications«, acronym BIOAD, https://bioad.ijs.si/ (grant No. J7-4639) and core funding (grants No. P2-0393 and No. P1-0134). Dr. Ana Kraš's valuable help in presenting EIS results is acknowledged. The XPS analysis was conducted at the Department of Surface Engineering of the Jožef Stefan Institute (Prof. Janez Kovač and Tatjana Filipič, MSc). The authors acknowledge the Centre of Excellence in Nanoscience and Nanotechnology-Nanocenter, Ljubljana, Slovenia, to access the scientific equipment, including FIB-SEM/EDXS.

ORCID

Ingrid Milošev https://orcid.org/0000-0002-7633-9954
Peter Rodič https://orcid.org/0000-0001-8664-0129

References

1. R. R. Boyer, “An overview on the use of titanium in the aerospace industry.” *Mat. Sci. Eng. A*, **213**, 103 (1996).
2. J. C. Williams and R. R. Boyer, “Opportunities and issues in the application of titanium alloys for aerospace components.” *Metals*, **10**, 705 (2020).
3. R. R. Boyer and R. D. Briggs, “The use of β titanium alloys in the aerospace industry.” *J. Mat. Eng. Perform.*, **14**, 681 (2000).
4. E. Marin and A. Lanzutti, “Biomedical applications of titanium alloys: a comprehensive review.” *Materials*, **17**, 114 (2023).
5. X. Liu, P. K. Chu, and C. Ding, “Surface modification of titanium, titanium alloys, and related materials for biomedical applications.” *Mat. Sci. Eng. R Rep.*, **47**, 49 (2004).
6. H. J. Rack and J. I. Qazi, “Titanium alloys for biomedical applications.” *Mat. Sci. Eng. C*, **26**, 1269 (2006).
7. M. Kulkarni, A. Mazare, E. Gongadze, Š. Perutkova, V. Kralj-Iglič, I. Milošev, P. Schmuki, A. Iglič, and M. Mozetič, “Titanium nanostructures for biomedical applications.” *Nanotechnology*, **26**, 062002 (2015).
8. M. Niinomi, “Mechanical biocompatibilities of titanium alloys for biomedical applications.” *J. Mech. Behav. Biomed. Mater.*, **1**, 30 (2008).
9. I. Gurrappa, “Characterization of titanium alloy Ti-6Al-4V for chemical, marine and industrial applications.” *Mater. Charact.*, **51**, 131 (2003).
10. S. Yan, G-L. Song, Z. Li, H. Wang, D. Zheng, F. Cao, M. Horynova, M. S. Dargusch, and L. Zhou, “A state-of-the-art review on passivation and biofouling of Ti and its alloys in marine environments.” *J. Mater. Sci. Technol.*, **34**, 421 (2018).
11. P. Pushp, S. M. Dasharath, and C. Arati, “Classification and applications of titanium and its alloys.” *Mater. Today Proc.*, **54**, 537 (2022).
12. S. L. D. Assis, S. Wolynec, and I. Costa, “2006. Corrosion characterization of titanium alloys by electrochemical techniques.” *Electrochim. Acta*, **51**, 1815 (2006).
13. I. Milošev, M. Metikoš-Huković, and H-H. Strehblow, “Passive film on orthopaedic TiAlV alloy formed in physiological solution investigated by X-ray photoelectron spectroscopy.” *Biomaterials*, **21**, 2103 (2000).
14. J. M. Cordeiro and V. A. R. Barão, “Is there scientific evidence favoring the substitution of commercially pure titanium with titanium alloys for the manufacture of dental implants?” *Mat. Sci. Eng. C*, **71**, 1201 (2017).
15. J. B. Brunski, “Chapter 2.9, "Metals"." *Biomaterials Science. An Introduction to Materials in Medicine*, ed. B. D. Ratner, A. S. Hoffman, F. J. Schoen, and J. E. Lemons et al. (Elsevier Academic Press, Cambridge, MA, USA) 2nd, ed., 137–153 (2004).
16. M. Noori, M. Atapour, F. Ashrafizadeh, H. Elmkhah, G. G. di Confiengo, S. Ferraris, S. Perero, M. Cardu, and S. Spriano, “Nanostructured multilayer CAE-PVD coatings based on transition metal nitrides on Ti6Al4V alloy for biomedical applications.” *Ceram. Int.*, **49**, 23367 (2023).
17. E. Mohseni, E. Zalnezhad, A. R. Bushroa, A. M. Hamouda, B. T. Goh, and G. H. Yoon, “Ti/TiN/HA coating on Ti–6Al–4V for biomedical applications.” *Ceram. Int.*, **41**, 14447 (2015).
18. T. R. Rautray, R. Narayanan, T-Y. Kwon, and K-H. Kim, “Surface modification of titanium and titanium alloys by ion implantation.” *J. Biomed. Mater. Res. B*, **93B**, 581 (2010).
19. C. K. Dyer and J. S. L. Leach, “Breakdown and efficiency of anodic oxide growth on titanium.” *J. Electrochem. Soc.*, **125**, 1032 (1978).
20. Y-T. Sul, C. B. Johansson, Y. Jeong, and T. Albrektsson, “The electrochemical oxide growth behaviour on titanium in acid and alkaline electrolytes.” *Med. Eng. Phys.*, **23**, 329 (2001).
21. A. Wisbey, P. J. Gregson, L. M. Peter, and M. Tuke, “Effect of surface treatment on the dissolution of titanium-based implant and materials.” *Biomaterials*, **12**, 470 (1991).
22. I. Milošev, “Chapter 1. “Surface treatments of titanium with microbacterial agents for implant applications,” In “Biomedical and Pharmaceutical Applications of Electrochemistry.” *Modern Aspects of Electrochemistry*, ed. S. Djokić (Springer, Berlin) 60, 1 (2016).
23. J. Alipal, N. A. S. Mohd Pu’ad, N. H. M. Nayan, N. Sahari, H. Z. Abdullah, M. I. Idris, and T. C. Lee, “An updated review on surface functionalisation of titanium and its alloys for implant applications.” *Mater. Today Proc.*, **42**, 270 (2021).
24. I. Milošev, T. Kosec, and H-H. Strehblow, “XPS and EIS study of the passive film formed on orthopaedic Ti-6Al-7Nb alloy in Hank’s physiological solution.” *Electrochim. Acta*, **53**, 3547 (2008).

25. I. Milošev, J. Hmeljak, G. Žerjav, A. Cör, J. M. Calderon Moreno, and M. Popa, "Quaternary Ti-20Nb-10Zr-5Ta alloy during immersion in simulated physiological solutions: formation of layers, dissolution and biocompatibility." *J. Mater. Sci. Mater. Med.*, **25**, 1099 (2014).
26. I. Milošev, G. Žerjav, J. M. Calderon Moreno, and M. Popa, "Electrochemical properties, chemical composition and thickness of passive film formed on novel Ti-20Nb-10Zr-5Ta alloy." *Electrochim. Acta*, **99**, 176 (2013).
27. T. D. Burleigh, "Oxides formed on titanium by polishing, etching, anodizing, or thermal oxidizing." *Corrosion*, **56**, 1233 (2000).
28. I. Milošev and B. Kapun, "The corrosion resistance of Nitinol alloy in simulated physiological solutions: I. The effect of surface preparation." *Mat. Sci. Eng. C*, **32**, 1087 (2012).
29. I. Milošev and B. Kapun, "The corrosion resistance of Nitinol alloy in simulated physiological solutions: II. The effect of surface treatment." *Mat. Sci. Eng. C*, **32**, 1068 (2012).
30. R. C. Souza, C. A. R. Maestro, S. L. M. Ribeiro Filho, S. Clemasco, B. A. F. Sanots, M. E. D. Serenário, A. M. De Sousa Malafaia, I. N. Bastos, L. C. Brandão, and A. H. S. Bueno, "Surface finishing and shape effects on corrosion resistance of Ti-6Al-4V alloy in the simulated body fluid." *Mat. Res.*, **25**, e20210546 (2022).
31. E. Dănăilă and L. Benea, "The effect of surface roughness on corrosion behaviour of Ti-6Al-4V in saliva solution." *The 5th IEEE International Conference on E-Health and Bioengineering EHB 2015, Iaşi* (2015), https://ieeexplore.ieee.org/abstract/document/7391518.
32. G. Chi, D. Yi, and H. Liu, "Effect of roughness on electrochemical and pitting corrosion of Ti-6Al-4V alloy in 12 wt% HCl solution at 35 °C." *J. Mater. Res. Technol.*, **9**, 1162 (2020).
33. Z. Cai, H. Nakajima, M. Woldu, A. Berglund, M. Bergman, and T. Okabe, "*In vitro* corrosion resistance of titanium made using different fabrication methods." *Biomaterials*, **20**, 183 (1999).
34. G. Chen, X. Wen, and N. Zhang, "Corrosion resistance and ion dissolution of titanium with different surface microroughness." *Bio-Med. Mater. Eng.*, **8**, 61 (1998).
35. X. Cheng and S. G. Roscoe, "Influence of surface polishing on the electrochemical behavior of titanium." *Electrochem. Solid-St. Letters*, **8**, B38 (2005).
36. C. Liang, W. Liu, S. Li, H. Kong, Z. Zhang, and S. Song, "A nano-scale mirror-like surface of Ti-6Al-4V attained by chemical mechanical polishing." *Chin. Phys. B*, **25**, 058301 (2016).
37. C. Deng, L. Jiang, N. Qin, and L. Qian, "Effects of pH and H_2O_2 on the chemical polishing of titanium alloys." *J. Mater. Process. Techol.*, **295**, 117204 (2021).
38. Z. Ozdemir, A. Ozdemir, and G. B. Basim, "Application of chemical mechanical polishing process on titanium based implants." *Mat. Sci. Eng. C*, **68**, 383 (2016).
39. Z. Zhang, Z. Shi, Y. Du, Z. Yu, L. Gua, and D. Guo, "A novel approach of chemical mechanical polishing for a titanium alloy using an environment-friendly slurry." *Appl. Surf. Sci.*, **427**, 409 (2018).
40. S. Okawa and K. Watanabe, "Chemical mechanical polishing of titanium with colloidal silica containing hydrogen peroxide – mirror polishing and surface properties." *Dent. Mater. J.*, **28**, 68 (2009).
41. J. M. Oh, B. G. Lee, S-W. Cho, S-W. Lee, G-S. Choi, and J-W. Lim, "Oxygen effects on the mechanical properties and lattice strain of Ti and Ti-6Al-4V." *Met. Mater. Int.*, **17**, 733 (2011).
42. Y. Chong et al., "Mechanistic basis of oxygen sensitivity in titanium." *Sci. Adv.*, **6**, eabc4060 (2020).
43. X. Gai, Y. Bai, S. Li, W. Hou, Y. Hao, X. Zhang, R. Yang, and R. D. K. Misra, "In-situ monitoring of the electrochemical behaviour of cellular structured biomedical Ti-6Al-4V alloy fabricated by electron beam melting in simulated physiological fluid." *Acta Biomater.*, **106**, 387 (2020).
44. I. D. Raistrick, J. R. MacDonald, and D. R. Franceschetti, *Impedance Spectroscopy Emphasizing Solid Materials and Systems* (John Wiley & Sons, New York) (1987).
45. P. J. Boddy, "Oxygen evolution on semiconducting TiO_2." *J. Electrochem. Soc.*, **115**, 199 (1968).
46. M. Metikoš-Huković, A. Kwokal, and J. Piljac, "The influence of niobium and vanadium on passivity of titanium-based implants in physiological solution." *Biomaterials*, **24**, 3765 (2003).
47. I. Milošev, B. Kapun, and V. S. Šelih, "The effect of fluoride ions on the corrosion behaviour of Ti metal, and Ti6-Al-7Nb and Ti-6Al-4V alloys in artificial saliva." *Acta Chim. Slov.*, **60**, 543 (2013), https://acsi-journal.eu/index.php/ACSi/article/view/88.
48. I. Milošev, "The effect of biomolecules on the behaviour of CoCrMo alloy in various simulated physiological solutions." *Electrochim. Acta*, **78**, 259 (2012).
49. P. Tengvall, H. Elwing, and I. Lundström, "Titanium gel made from metallic titanium and hydrogen perodixe." *J. Colloid Interface Sci.*, **130**, 405 (1989).
50. I. Spajić, P. Rodič, G. Šekularac, M. Lekka, L. Fedrizzi, and I. Milošev, "The effect of surface preparation on the protective properties of Al_2O_3 and HfO_2 thin films deposited on cp-titanium by atomic layer deposition." *Electrochim. Acta*, **366**, 137431 (2021).